Correspondence to:
F. Němec,
frantisek.nemec@gmail.com

Enhanced ionization of the Martian nightside ionosphere during solar energetic particle events

F. Němec[1], D. D. Morgan[2], C. Diéval[2], D. A. Gurnett[2], and Y. Futaana[3]

[1]Faculty of Mathematics and Physics, Charles University in Prague, Prague, Czech Republic, [2]Department of Physics and Astronomy, University of Iowa, Iowa City, Iowa, USA, [3]Swedish Institute of Space Physics, Kiruna, Sweden

Abstract Electron densities in the Martian nightside ionosphere are more than 90% of time too low to be detected by the Mars Advanced Radar for Subsurface and Ionosphere Sounding radar sounder on board the Mars Express spacecraft. However, the relative number of ionograms with peak electron density high enough to be detected represents a good statistical proxy of the ionospheric density. We focus on solar energetic particle (SEP) events, and we analyze their effects on ionospheric formation. SEP time intervals were identified in situ using the background counts recorded by the ion sensor of the ASPERA-3 instrument on board Mars Express. We show that peak electron densities during the SEP events are large enough to be detected in more than 30% of measurements, and, moreover, the reflections of the sounding signal from the ground almost entirely disappear. Nightside electron densities during SEP events are thus substantially increased as compared to normal nightside conditions.

1. Introduction

Electron densities in the nightside ionosphere of Mars are often below the detection thresholds of employed experimental methods. Moreover, radio occultation measurements are restricted to solar zenith angles (SZAs) lower than about 132° because of geometric constraints imposed by the orbits of Earth and Mars. This significantly limits the number of available nightside ionospheric observations and our understanding of the Martian nightside in general. Two main mechanisms which are likely to contribute to the ionospheric formation are plasma transport from the dayside and electron precipitation [*Fox et al.*, 1993].

When detectable (about 40% of the analyzed electron density profiles), nightside peak electron densities determined from Viking radio occultation measurements were on the order of 5×10^3 cm^{-3} at peak altitudes of about 150 km [*Zhang et al.*, 1990]. Surface echoes measured by Mars Advanced Radar for Subsurface and Ionospheric Sounding (MARSIS) on board the Mars Express spacecraft were used by *Safaeinili et al.* [2007] to determine the total electron content (TEC). Their results indicated higher TECs in nightside regions where the crustal magnetic field was nearly vertical, which is likely to be a consequence of the connection between the interplanetary and the crustal magnetic fields. *Withers et al.* [2012] examined electron density profiles from occultation measurements performed by the Mars Express Radio Science Experiment (MaRS). They underlined the importance of plasma transport from the dayside up to SZA ≈ 115°. Electron precipitation is likely to be a dominant source at higher SZAs, and the observed peak altitudes of about 130–170 km are consistent with recent modeling efforts [*Fillingim et al.*, 2007; *Lillis et al.*, 2009, 2011].

Withers et al. [2012] also reported that solar energetic particle (SEP) events can be the main source of nightside plasma, causing ionization at peak altitudes much lower than usual (≈ 90 km). SEP-produced secondary electrons were detected by Mars Global Surveyor (MGS) [*Lillis et al.*, 2012]. Because of low ionization altitudes, SEP events significantly increase the absorption coefficient of propagating electromagnetic waves due to electron-neutral collisions [*Withers*, 2004]. The absorption can eventually become large enough to prevent the MARSIS sounding signal reflected from the planetary surface to be detected [*Morgan et al.*, 2006; *Espley et al.*, 2007]. Theoretical investigations of SEP effects indicate that for a reasonably strong SEP event, the ionospheric response should be readily observable [*Leblanc et al.*, 2002; *Sheel et al.*, 2012]. The effects of SEP events on the Martian dayside ionosphere were experimentally analyzed by *Ulusen et al.* [2012] using the MGS Radio Science (RS) experiment. They found no clear evidence for an increase in the ionospheric density between 100 and 200 km and pointed out that a possible reason may be that the extra ionization produced by SEP events is below 80 km, which is out of the coverage of the RS profiles.
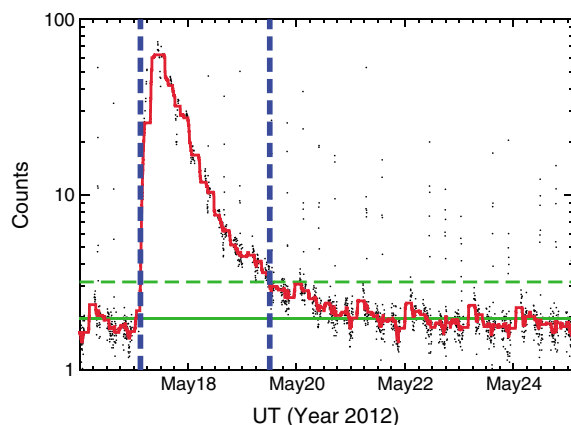
Figure 1. Example of a SEP event determined using the background counts data recorded by the IMA sensor. The data were measured in 2012, and the appropriate dates are marked on the abscissa axis. The measured number of background counts is shown by the black points. The red curve corresponds to the median filtered data. The vertical blue lines mark the time interval corresponding to the SEP event. The mean nominal counts value and the appropriate threshold value are shown by the horizontal green solid and dashed lines, respectively (see text for more details).

We report results of a survey of the Martian nightside ionosphere observed by MARSIS during the times of SEP events. These are determined in situ, and their importance for the ionospheric formation is demonstrated. The obtained results have important consequences both for the nightside modeling effort and for radio wave propagation.

2. Data Set

Data acquired by the Mars Express spacecraft have been used [*Chicarro et al.*, 2004]. Among different instruments on board, we have used data from the Analyzer of Space Plasma and Energetic Atoms (ASPERA-3) instrument [*Barabash et al.*, 2006] and from the MARSIS radar sounder [*Picardi et al.*, 2004; *Gurnett et al.*, 2005; *Jordan et al.*, 2009; *Morgan et al.*, 2013].

Although the energy range of the Ion Mass Analyzer (IMA) sensor of the ASPERA-3 instrument does not allow direct measurements of SEPs, the number of counts in the highest-energy channels can be used as a proxy for high-energy particles penetrating the instrument and reaching the detectors [*Capalbo*, 2010; *Delory et al.*, 2012]. The energy of the penetrating particles is related to the housing of the instrument and should be larger than about 30 MeV. Case studies of multipoint multi-instrumental data revealed that several days long, large increases in background counts (BKGCs) are caused by increased high-energy particle fluxes during SEP events [*Futaana et al.*, 2008; *Frahm et al.*, 2013]. An example of the BKGCs variation during an SEP event is shown by the black points in Figure 1. As there is a significant scatter in the BKGCs data, and some individual data points are well off the expected smooth variation, we have applied a median filter over the 20 nearest neighboring data points in order to get a more representative trend. The filtered data are shown by the red curve, and it will be these filtered data that we will use as a proxy for the energetic particle flux at a given time. This allows us not only to identify the time intervals of individual SEP events but also to compare their respective strengths.

Periods with BKGCs visibly increasing above normal levels (hereinafter referred to as SEP events) were manually identified in all BKGCs data recorded by IMA during the time intervals with MARSIS nightside ionospheric sounding data available. The exact beginning and ending times of SEP events were determined by an automatic threshold-using procedure. As nominal BKGCs are caused by galactic cosmic rays, and have a slight variation over the solar cycle, the used threshold value was different for each of the events, based on data measured during 60 days centered on the time of the maximum BKGCs. We considered only BKGCs lower than 5 (which is the upper estimate of the nominal counts value), and we defined the threshold value as 3 standard deviations above mean. Note that although this procedure is in principle able to identify SEP events Automatically, a manual verification of all identified events was used to eliminate false alarms. The results of the procedure applied to the example event are shown in Figure 1. The mean nominal counts value is shown by the horizontal solid green line, and the appropriate threshold is shown by the horizontal dashed green line. The time interval of the SEP event is marked by the blue vertical lines. The list of 15 SEP events that we have identified is given in Table 1. Mean nominal counts for these events varied from about 1.6 to 3, and threshold values varied from about 3 to 5.2.

The MARSIS instrument for topside ionospheric sounding uses sounding frequencies from 0.1 to 5.5 MHz. This theoretically corresponds to detectable peak electron densities from about 124 cm^{-3} to 3.75×10^5 cm^{-3}. However, since the radiated power falls off rapidly at sounding frequencies below about 500 kHz, it is usually not possible to detect peak electron densities lower than about 5000 cm^{-3}. Note that this threshold is only approximate, and the actual value may vary from case to case, depending on the amount of noise in the ionogram and other relevant conditions [see *Němec et al.*, 2010, Figure 6a]. Nevertheless, the information about whether or not the peak electron density is large enough to be detected by MARSIS can still be used

Table 1. List of SEP Time Intervals[a]

Start Time	End Time	Max(Counts)
2006-12-05 12:24	2006-12-10 23:34	123.16
2011-03-08 05:53	2011-03-08 16:08	8.86
2011-06-05 02:56	2011-06-09 17:33	229.00
2011-07-12 10:43	2011-07-12 15:37	5.75
2011-09-22 16:25	2011-09-23 13:21	13.27
2012-01-23 16:54	2012-01-27 04:10	30.86
2012-01-27 18:56	2012-02-01 17:42	479.82
2012-03-07 05:59	2012-03-16 02:28	338.84
2012-05-17 02:56	2012-05-19 12:10	62.73
2012-07-18 09:17	2012-07-18 16:11	8.32
2012-07-26 08:01	2012-07-27 05:45	9.89
2012-08-31 22:57	2012-09-03 17:08	10.93
2012-09-28 01:24	2012-09-28 11:18	3.89
2013-03-05 10:08	2013-03-08 11:19	21.50
2013-05-13 17:33	2013-05-14 11:06	8.36

[a]Only the time intervals with MARSIS nightside ionospheric sounding data available were selected. Maximum number of background counts, which serves as a proxy for high-energy particle flux, is provided for each of the events. Dates are formatted as year-month-day.

in a statistical way to characterize the electron density in the ionosphere [*Němec et al.*, 2010]. Moreover, if the peak electron density is large enough to be detected, it can be readily determined from the maximum frequency of the ionospheric reflection. Unfortunately, as the nightside ionospheric reflections are typically oblique [*Gurnett et al.*, 2008; *Němec et al.*, 2011], they cannot be used to determine peak altitudes.

We use the same approach as *Němec et al.* [2010]. Only data measured at SZA $>$ 107° were used to ensure that the ionosphere at the expected peak altitude of $\approx$ 150 km [*Fillingim et al.*, 2007] is in the shadow of the planet. Further, only data measured at altitudes lower than 1100 km were selected to ensure that an ionospheric echo—if present—would be within the time delay sampled by MARSIS. Altogether, 3092 MARSIS ionograms that satisfy the aforementioned two conditions were measured during the times of SEP events from Table 1. All these ionograms were visually inspected for the presence of ionospheric and surface reflections. Ionospheric reflections occurred in 817 ionograms ($\approx$ 26%), meaning that the peak electron density in the remaining 2275 ionograms was too low to be detected. Surface reflections occurred in 672 ionograms ($\approx$ 22%), meaning that the sounding signal in the remaining 2420 ionograms was too attenuated during the ionospheric propagation to receive a detectable reflection from the surface.

3. Results

The ratio of the number of ionograms with peak electron density large enough to be detected to the total number of inspected ionograms as a function of the number of BKGCs recorded by IMA is shown in Figure 2 by the black line. The ratio of the number of ionograms with the attenuation of the sounding signal low enough for the surface reflection to be detected to the total number of inspected ionograms is shown by the blue line. The error bars at each individual bin are upper estimates calculated assuming the binomial distribution (i.e., $\sigma = 0.5/\sqrt{N}$, where N is the number of inspected ionograms in a given bin). It can be seen that the occurrence rate of ionograms with ionospheric reflections systematically increases with the number of BKGCs, from less than 0.2 for no-SEP/weak-SEP time intervals up to more than 0.6 for strong-SEP time intervals. This should be contrasted with the long-term occurrence rate of nightside ionograms with ionospheric reflections determined using more than 4 years of data, which is less than 10% [*Němec et al.*, 2010]. The occurrence rate of ionograms with surface reflections systematically decreases with the number of background counts. Virtually no surface reflections are detected during strong-SEP time intervals.

Němec et al. [2010] reported that about 90% of nightside ionospheres have peak electron density lower than 5000 cm^{-3}, and only less than 2% of the events have peak electron densities larger than 1.9 $\times$ 10^4 cm^{-3}. However, during the SEP time intervals, the

Figure 2. Relative number of MARSIS ionograms with peak electron density large enough to be detected as a function of the number of background counts recorded by the IMA sensor (black). Relative number of MARSIS ionograms with the attenuation of the sounding signal low enough for the surface reflection to be detected (blue). The error bars were calculated assuming the binomial distribution, taking into account the number of ionograms that fall in a given bin.
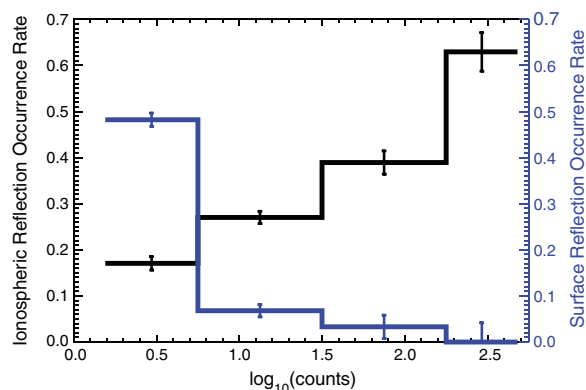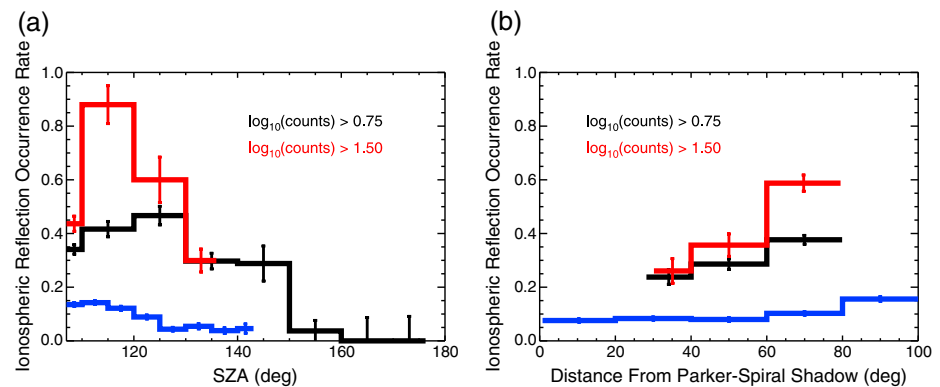
Figure 3. Relative number of MARSIS ionograms with peak electron density large enough to be detected as a function of (a) solar zenith angle and (b) distance from the idealized Parker-spiral magnetic shadow (see text). Two different background count thresholds were employed, namely, $\log_{10}(counts) > 0.75$ (black curve) and $\log_{10}(counts) > 1.50$ (red curve). The long-term average dependence obtained by *Němec et al.* [2010] is overplotted by the blue line for comparison. The error bars were calculated assuming the binomial distribution, taking into account the number of ionograms that fall in a given bin.

percentage of nightside ionospheres with peak electron density lower than 5000 cm^{-3} decreases to about 75%, while more than 5% of nightside ionospheres have peak electron densities larger than 1.9×10^4 cm^{-3}. Taking into account only the time intervals with $\log_{10}(counts) > 1.5$, i.e., the strong-SEP time intervals corresponding to the last two bins of Figure 2, we find that the percentage of nightside ionospheres with peak electron density lower than 5000 cm^{-3} decreases to less than 60%, while the peak electron density is larger than 1.9×10^4 cm^{-3} in nearly 10% of cases. This clearly demonstrates that SEP events have a major influence on the formation of the nightside ionosphere.

The relative number of MARSIS ionograms with peak electron density large enough to be detected as a function of SZA is plotted in Figure 3a. The results were obtained by considering only SEP time intervals with the number of BKGCs larger than a threshold value, namely $\log_{10}(counts) > 0.75$ for the black line, and $\log_{10}(counts) > 1.5$ for the red line. The long-term average occurrence rate of ionospheric reflections as a function of SZA obtained by *Němec et al.* [2010] is overplotted by the blue line for comparison. It appears that the ionospheric reflection occurrence rate at high SZAs is extremely low. However, it should be emphasized that the amount of data measured at such large SZAs is very limited, and, moreover, all of them were obtained during the periods of not very high values of BKGCs.

While the bulk of the solar wind streams radially straight from the Sun, the paths of more energetic particles are dominated by gyromotion around interplanetary magnetic field (IMF) lines. The average direction of the IMF at Mars is in the ecliptic plane and at 57° to the Mars-Sun line. The degree to which this will result in magnetic shadow behind the planet along the direction of the IMF is a function of the pitch angle isotropy of the SEP distribution and the energy (and hence gyroradius) of the particles [*Luhmann et al.*, 2007]. Distributions beamed along the IMF direction will result in significant shadowing while more isotropic distributions, particularly at high energies, will result in less shadowing as particles should hit the planet (including the nightside) from the front and side. Although some extensive modeling of this effect has been done [*Kallio et al.*, 2012; *McKenna-Lawlor et al.*, 2012], we limit ourselves to analyzing the dependence on a distance from the average Parker spiral shadow location in degrees. The obtained results are shown in Figure 3b, using the same format as in Figure 3a. It can be seen that while the ionospheric reflection occurrence rate close to the magnetic shadow is about 25%, it increases up to nearly 40% well away from the magnetic shadow for SEP time intervals with $\log_{10}(counts) > 0.75$ and up to about 60% for SEP time intervals with $\log_{10}(counts) > 1.5$. The long-term average occurrence rate based on *Němec et al.* [2010] data is overplotted by the blue line for comparison. An increasing trend is found also in this long-term data, which shows that the impact ionization by high-energy particles streaming along the IMF is important also for the long-term average ionization in the nightside ionosphere.

4. Discussion and Conclusions

Although SEP events might play a significant role already on the dayside, their importance increases even further on the nightside, where the electron density is much lower, and any additional ionization is therefore

much more important. The analysis of BKGCs recorded by the IMA sensor allowed us to determine the time intervals corresponding to SEP events in situ and, moreover, to obtain a proxy for the high-energy particle flux at Mars Express at any time of interest. Although the electron density in the ionosphere was often below the detection threshold of the MARSIS instrument, it could still be evaluated in a statistical sense.

Figure 2 shows that the relative number of ionograms with peak electron densities large enough to be detected increases with the high-energy particle flux proxy and is significantly larger than the long-term average reported by *Němec et al.* [2010]. This, along with the analysis of peak electron densities, demonstrates the importance of SEP events for nightside ionospheric formation. The attenuation of the sounding signal is so large that the surface reflections during the periods of well-pronounced SEP events become virtually undetectable. This implies a one-way attenuation larger than about 13 dB [*Nielsen et al.*, 2007]. Taking into account that nightside peak electron densities are typically on the order of 5000 cm^{-3}, and the MARSIS sounding frequency extends up to 5.5 MHz, the altitudes where the ionization takes place can be at least roughly estimated using the attenuation calculations reported by *Withers* [2004]. Namely, *Withers* [2004, Figure 3] suggests that a significant ionization should take place below about 80 km in order to explain the observed attenuation. However, this does not exclude a possibility of a significant ionization also above this altitude. In fact, the results of *Lillis et al.* [2012] are only consistent with substantial SEP-produced ionization above 150 km. SEP events therefore seem to produce ionization at a large range of altitudes, being consistent with a large range of SEP energies and simulation results obtained by *Sheel et al.* [2012, Figures 5 and 6].

BKGCs recorded by the IMA sensor used as the proxy for the high-energy particle flux appear to be the main controlling factor of the Martian nightside ionospheric formation. This complicates the analysis of the dependence on other parameters. Namely, the data measured during various levels of high-energy particle fluxes are necessarily mixed together in Figure 3. Especially in the case of SZA dependence, we are not able to distinguish whether the low ionospheric reflection occurrence rate at large SZAs is not due to low BKGCs during the relevant periods, rather than due to the SZA dependence. However, the larger occurrence rate of ionospheric reflections at lower SZAs may be related to the plasma transport from the dayside. This is considered to be an important source of the nightside ionization near the terminator [*Němec et al.*, 2010; *Withers et al.*, 2012], and it is likely to be further enhanced during SEP events, because the SEP impact ionization creates additional ions available for transport.

Our main results can be summarized as follows: (i) We have used BKGCs data recorded by the IMA sensor on board Mars Express as a proxy for high-energy particle flux and compiled a list of 15 SEP events that occurred at times of MARSIS nightside measurements. (ii) We have analyzed the occurrence rate of both ionospheric reflections and surface reflections at the times of SEP events, demonstrating that the nightside ionosphere during these periods is extremely enhanced as compared to normal conditions. (iii) A significant ionization is likely to take place below about 80 km, and there is an evidence for the magnetic shadow effect in our data. These results clearly show that electron densities in the Martian nightside ionosphere under the influence of SEP events are vastly different from those under normal conditions.

References

Barabash, S., et al. (2006), The analyzer of space plasmas and energetic atoms (ASPERA-3) for the Mars Express mission, *Space Sci. Rev.*, *126*, 113–164, doi:10.1007/s11214-006-9124-8.

Capalbo, F. J. (2010), Background analysis for IMA sensor on ASPERA instrument, *IRF Technical Report 54*, IRF, Kiruna, Sweden.

Chicarro, A., P. Martin, and R. Trautner (2004), The Mars Express mission: An overview, in *Mars Express: The Scientific Payload*, vol. 1240, edited by A. Wilson and A. Chicarro, pp. 3–13, ESA Special Publication ESTEC, Noordwijk, Netherlands.

Delory, G. T., J. G. Luhmann, D. Brain, R. J. Lillis, D. L. Mitchell, R. A. Mewaldt, and T. V. Falkenberg (2012), Energetic particles detected by the electron reflectometer instrument on the Mars Global Surveyor, 1999–2006, *Adv. Space Res.*, *10*, S06003, doi:10.1029/2012SW000781.

Espley, J. R., W. H. Farrell, D. A. Brain, D. D. Morgan, B. Cantor, J. J. Plaut, M. H. Acuña, and G. Picardi (2007), Absorption of MARSIS radar signals: Solar energetic particles and the daytime ionosphere, *J. Geophys. Res.*, *34*, L09101, doi:10.1029/2006GL028829.

Fillingim, M. O., L. M. Peticolas, R. J. Lillis, D. A. Brain, J. S. Halekas, D. L. Mitchell, R. P. Lin, D. Lummerzheim, S. W. Bougher, and D. L. Kirchner (2007), Model calculations of electron precipitation induced ionization patches on the nightside of Mars, *Geophys. Res. Lett.*, *34*, L12101, doi:10.1029/2007GL029986.

Fox, J. L., J. F. Brannon, and H. S. Porter (1993), Upper limits to the nightside ionosphere of Mars, *Geophys. Res. Lett.*, *20*(13), 1339–1342.

Frahm, R. A., J. R. Sharber, J. D. Winningham, H. A. Elliott, T. A. Howard, C. E. DeForest, D. Odstrčil, E. Kallio, S. McKenna-Lawlor, and S. Barabash (2013), Solar energetic particle arrival at Mars due to the 27 January 2012 solar storm, *AIP Conf. Proc.*, *1539*(394–397), doi:10.1063/1.4811068.

Futaana, Y., et al. (2008), Mars Express and Venus Express multi-points observations of geoeffective solar flare events in December 2006, *Planet. Space Sci.*, *56*, 873–880.

Gurnett, D. A., et al. (2005), Radar soundings of the ionosphere of Mars, *Science*, *310*, 1929–1933.

Gurnett, D. A., et al. (2008), An overview of radar soundings of the martian ionosphere from the Mars Express spacecraft, *Adv. Space Res.*, *41*, 1335–1346.

Jordan, R., et al. (2009), The Mars Express MARSIS sounder instrument, *Planet. Space Sci.*, *57*, 1975–1986, doi:10.1016/j.pss.2009.09.016.

Kallio, E., S. McKenna-Lawlor, M. Alho, R. Jarvinen, S. Dyadechkin, and V. V. Afonin (2012), Energetic protons at Mars: Interpretation of SLED/Phobos-2 observations by a kinetic model, *Ann. Geophys.*, *30*, 1595–1609, doi:10.5194/angeo-30-1595-2012.

Leblanc, F., J. G. Luhmann, R. E. Johnson, and E. Chassefiere (2002), Some expected impacts of a solar energetic particle event at Mars, *J. Geophys. Res.*, *107*(A5), 1058, doi:10.1029/2001JA900178.

Lillis, R. J., M. O. Fillingim, L. M. Peticolas, D. A. Brain, R. P. Lin, and S. W. Bougher (2009), Nightside ionosphere of Mars: Modeling the effects of crustal magnetic fields and electron pitch angle distributions on electron impact ionization, *J. Geophys. Res.*, *114*, E11009, doi:10.1029/2009JE003379.

Lillis, R. J., M. O. Fillingim, and D. A. Brain (2011), Three-dimensional structure of the Martian nightside ionosphere: Predicted rates of impact ionization from Mars Global Surveyor magnetometer and electron reflectometer measurements of precipitating electrons, *J. Geophys. Res.*, *116*, A12317, doi:10.1029/2011JA016982.

Lillis, R. J., D. A. Brain, G. T. Delory, D. L. Mitchell, J. G. Luhmann, and R. P. Lin (2012), Evidence for superthermal secondary electrons produced by SEP ionization in the Martian atmosphere, *J. Geophys. Res.*, *117*, E03004, doi:10.1029/2011JE003932.

Luhmann, J. G., C. Zeitlin, R. Turner, D. A. Brain, D. Delory, J. G. Lyon, and W. Boynton (2007), Solar energetic particles in near-Mars space, *J. Geophys. Res.*, *112*, E10001, doi:10.1029/2006JE002886.

McKenna-Lawlor, S., E. Kallio, R. Jarvinen, and V. V. Afonin (2012), Magnetic shadowing of high energy ions at Mars and how this effect can be simulated using a hybrid model, *Earth Planets Space*, *64*, 247–256.

Morgan, D. D., D. A. Gurnett, D. L. Kirchner, R. L. Huff, D. A. Brain, W. V. Boynton, M. H. Acuña, J. J. Plaut, and G. Picardi (2006), Solar control of radar wave absorption by the Martian ionosphere, *Geophys. Res. Lett.*, *33*, L13202, doi:10.1029/2006GL026637.

Morgan, D. D., O. Witasse, E. Nielsen, D. A. Gurnett, F. Duru, and D. L. Kirchner (2013), The processing of electron density profiles from the Mars Express MARSIS topside sounder, *Radio Sci.*, *48*(3), 197–207, doi:10.1002/rds.20023.

Nielsen, E., D. D. Morgan, D. L. Kirchner, J. Plaut, and G. Picardi (2007), Absorption and reflection of radio waves in the Martian ionosphere, *Planet. Space Sci.*, *55*, 864–870.

Němec, F., D. D. Morgan, D. A. Gurnett, and F. Duru (2010), Nightside ionosphere of Mars: Radar soundings by the Mars Express spacecraft, *J. Geophys. Res.*, *115*, E12009, doi:10.1029/2010JE003663.

Němec, F., D. D. Morgan, D. A. Gurnett, and D. A. Brain (2011), Areas of enhanced ionization in the deep nightside ionosphere of Mars, *J. Geophys. Res.*, *116*, E06006, doi:10.1029/2011JE003804.

Picardi, G., et al. (2004), MARSIS: Mars advanced radar for subsurface and ionosphere sounding, in *Mars Express: The Scientific Payload*, vol. 1240, edited by A. Wilson and A. Chicarro, pp. 51–69, ESA Special Publication ESTEC, Noordwijk, Netherlands.

Safaeinili, A., W. Kofman, J. Mouginot, Y. Gim, A. Herique, A. B. Ivanov, J. J. Plaut, and G. Picardi (2007), Estimation of the total electron content of the Martian ionosphere using radar sounder surface echoes, *Geophys. Res. Lett.*, *34*, L23204, doi:10.1029/2007GL032154.

Sheel, V., S. A. Haider, P. Withers, K. Kozarev, I. Jun, S. Kang, G. Gronoff, and C. S. Wedlund (2012), Numerical simulation of the effects of a solar energetic particle event on the ionosphere of Mars, *J. Geophys. Res.*, *117*, A05312, doi:10.1029/2011JA017455.

Ulusen, D., D. A. Brain, J. G. Luhmann, and D. L. Mitchell (2012), Investigation of Mars' ionospheric response to solar energetic particle events, *J. Geophys. Res.*, *117*, A12306, doi:10.1029/2012JA017671.

Withers, P. (2004), Attenuation of radio signals by the ionosphere of Mars: Theoretical development and application to MARSIS observations, *Radio Sci.*, *46*, RS2004, doi:10.1029/2010RS004450.

Withers, P., et al. (2012), Observations of the nightside ionosphere of Mars by the Mars Express Radio Science Experiment (MaRS), *J. Geophys. Res.*, *117*, A12307, doi:10.1029/2012JA018185.

Zhang, M. H. G., J. G. Luhmann, and A. J. Kliore (1990), An observational study of the nightside ionospheres of Mars and Venus with radio occultation methods, *J. Geophys. Res.*, *95*(A10), 17,095–17,102.